JOURNAL OF MAGNETIC RESONANCE **135,** 118–125 (1998)
ARTICLE NO. MN981559

Mobility and Free Radical Concentration Effects in Proton–Electron Double-Resonance Imaging

Paulo L. de Sousa,* Ricardo E. de Souza,* Mario Engelsberg,* and Luiz A. Colnago†

**Departamento de Física, Universidade Federal de Pernambuco, Recife, Pernambuco, Brazil; and †Empresa Brasileira de Pesquisa Agropecuária (EMBRAPA—Instrumentação Agropecuária), São Carlos, São Paulo, Brazil*

Received August 29, 1997; revised July 23, 1998

The dependence of the enhancement of proton–electron double-resonance images upon the mobility of the proton bearing molecules, of the concentration of free radicals, and of the pulsed saturating RF power is studied in a magnetic field of 16 mT. The data exhibit a behavior which, in the potentially interesting region of small free radical concentration, may differ substantially from the high-concentration regime depending upon experimental conditions. The results permit a clearer understanding of the factors determining enhancement and contrast in images obtained by dynamic nuclear polarization. © 1998 Academic Press

Key Words: **Overhauser imaging; PEDRI; DNP; MRI; enhancement; mobility.**

I. INTRODUCTION

The possibility of taking advantage of the enhancement available through dynamic nuclear polarization (DNP) via the Overhauser effect for ^{1}H NMR imaging at very low magnetic fields has attracted considerable interest in recent years (*1–5*). Although several problems remain unresolved, especially concerning potential biological or medical applications, none of these problems appear to be completely insurmountable and an intensive effort to overcome some of the obstacles is in progress.

One aspect which deserves special attention is the understanding of the factors which determine enhancement and contrast in proton–electron double-resonance imaging (PEDRI). In normal magnetic resonance imaging (MRI), T_1 and T_2 contrasts are determined by the spectral densities of the fluctuating ^{1}H–^{1}H dipolar fields modulated by random molecular motion. T_1 contrast, for example, is sensitive to differences in spectral weights at the proton Larmor frequency. In the case of PEDRI, the spectral density function of the electron–proton interaction plays a major role. Overhauser enhancement in free radical solutions can be appreciable only when molecular motion takes place in a time scale which is fast or comparable with the inverse electronic Larmor frequency, which is almost three orders of magnitude larger than the nuclear Larmor frequency. Hence, contrast in PEDRI is expected to depend upon molecular mobility in a quite different manner than conventional MRI in the same value of magnetic field.

Although the basic principles which determine the effect of molecular motion upon Overhauser enhancement are quite well established (*6, 7*), the competing requirements peculiar to PEDRI in low magnetic fields seem to justify some reexamination. Nicholson *et al.* (*8*) have recently studied this problem and determined parameters which describe the image dependence on viscosity in glycerol–water mixtures. A large reduction of the enhancement was observed in a 2 mM free radical concentration, as the viscosity increased from $\eta = 1$ cP (pure water) to $\eta = 60$ cP (71% glycerol/29% water by volume at 24°C). In this paper we present the results of measurements of Overhauser enhancement performed over a range of concentrations, viscosities, and saturating RF power in glycerol–water mixtures. Our results suggest that, at low concentrations of free radical, the behavior differs from that reported in Ref. (*8*) and appears to be somewhat less restrictive, regarding the accessibility of slower molecular motions, than expected from measurements performed in the high-concentration regime. Furthermore, the role of the timing of the saturating pulse as an operational parameter for controlling contrast in PEDRI images at low radical concentrations is examined.

II. THEORY

The effect of molecular mobility upon enhancement of the NMR signal through DNP has been studied by several authors (*6–8*). The basic conclusions can be obtained by the procedure employed to derive Solomon's equations (*9*). If one considers, instead of a single nuclear spin as in Ref. (*9*), a pair of ^{1}H nuclei ($I = 1/2$) belonging to the solvent molecule with couplings to an unpaired electron spin $S = 1/2$ of a dissolved free radical, the following expression (*6*) for the enhancement E can be derived,

$$E = \langle I_z \rangle / I_0 = 1 - \rho f s |\gamma_s| / \gamma_I, \qquad [1]$$

where $\langle I_z \rangle$ denotes the expectation value of the dynamic nuclear polarization, I_0 is its thermal equilibrium value, s denotes the saturation parameter, and γ_s and γ_I are, respectively, electronic and nuclear gyromagnetic ratios. In the extreme narrow-

1090-7807/98 $25.00

ing limit, when the inverse electronic Larmor frequency is larger than the characteristic correlation time of the molecular motion, the coupling parameter ρ can be shown to have a value of $+0.5$ for dipolar electron–nucleus interactions and a value of -1 for purely scalar couplings (*6*).

The leakage factor f in Eq. [1] accounts for the loss of dynamic polarization caused by spin–lattice relaxation of nuclei within the solvent molecules via proton–proton dipolar couplings. It is therefore sensitive to the motion depending also upon the concentration of free radicals. It can be expressed in a relatively simple manner as (*6, 7*)

$$f = 1 - T_1/T_{10}, \qquad [2]$$

where $1/T_1$ denotes the total nuclear spin–lattice relaxation rate consisting of a sum of the free radical contribution and the intrinsic nuclear relaxation rate of the solvent molecules denoted by $1/T_{10}$.

If the condition for extreme narrowing is not satisfied, it can be more convenient to combine the product of the coupling parameter and the leakage factor into a single expression which will be shown to display explicitly the departure of the enhancement from the extreme narrowing value. For purely dipolar electron–nucleus interactions this product can be written as

$$\rho f = (W_2 - W_0)/(W_2 + W_0 + 2W_1 + 2\nu_1 + 2\nu_2). \qquad [3]$$

Here W_M ($M = 0, 1, 2$) denote transition probabilities per unit time caused by terms in the electron–nucleus dipole–dipole interaction randomly modulated by the molecular motion. They are labeled according to the change in the total magnetic quantum number $M = m_I + m_s$. Thus W_0 corresponds to $\Delta M = 0$, W_1 to $|\Delta M| = 1$ (but $\Delta m_s = 0$), and W_2 to $|\Delta M| = 2$. Similarly, the terms ν_m ($m = 1, 2$) represent transition probabilities per unit time caused by terms in the nuclear dipole–dipole interaction with $|\Delta m_I| = 1$ or 2, respectively.

The nuclear spin–lattice relaxation times of Eq. [2] are simply related to the transition probabilities of Eq. [3] (*9*). Thus $1/T_1 - 1/T_{10} = R(\omega) = W_2 + W_0 + 2W_1$ and $1/T_{10} = 2(\nu_1 + \nu_2)$, where we have introduced the radical-induced relaxation rate $R(\omega)$, expected to be proportional to the concentration of free radicals (*10*).

When the molecular motion is not fast enough for the extreme narrowing condition to hold, it is necessary to introduce correlation functions $J^{(M)}(\omega)$ and $\mathbb{J}^{(m)}(\omega)$ for the electron–nucleus and nucleus–nucleus dipole–dipole interactions, respectively. It is also convenient to introduce reduced spectral density functions for the motion defined as $j(\omega) = J^{(M)}(\omega)/J^{(M)}(0)$ and $\mathrm{j}(\omega) = \mathbb{J}^{(m)}(\omega)/\mathbb{J}^{(m)}(0)$, respectively. Moreover, if the relevant correlation time, albeit long compared with the inverse electronic Larmor frequency, is still short compared with the inverse proton Larmor frequency, the following approximations are possible for the values of the correlation functions $J^{(M)}(\omega)$ and $\mathbb{J}^{(m)}(\omega)$:

$$J^{(0)}(\omega_I - \omega_S) \cong J^{(0)}(\omega_S), \quad J^{(1)}(\omega_I) \cong J^{(1)}(0),$$
$$J^{(2)}(\omega_I + \omega_S) \cong J^{(2)}(\omega_S), \qquad [4a]$$
$$\mathbb{J}^{(1)}(\omega_I) \cong \mathbb{J}^{(1)}(0), \quad \mathbb{J}^{(2)}(2\omega_I) \cong \mathbb{J}^{(2)}(0). \qquad [4b]$$

$\omega_S/2\pi$ in Eqs. [4] denotes the electronic Larmor frequency whereas $\omega_I/2\pi$ denotes the much smaller nuclear Larmor frequency. For the glycerol–water mixtures used in our experiments at room temperature and very low magnetic fields, the assumption of an extreme narrowing condition with respect to ω_I in Eqs. [4] can be considered to be a good approximation although it may not hold for more viscous fluids or high magnetic fields.

With the approximations of Eqs. [4], the transition probabilities of Eq. [3] can be written in terms of their corresponding dipolar spectral density functions as (*10*)

$$W_0 \approx \gamma_I^2\gamma_s^2\hbar^2 S(S+1)(1/12)J^{(0)}(0)j(\omega_s) \qquad [5a]$$
$$W_1 \approx \gamma_I^2\gamma_s^2\hbar^2 S(S+1)(3/4)J^{(1)}(0) \qquad [5b]$$
$$W_2 \approx \gamma_I^2\gamma_s^2\hbar^2 S(S+1)(3/4)J^{(2)}(0)j(\omega_s), \qquad [5c]$$

with $J^{(0)}(0):J^{(2)}(0):J^{(1)}(0) = 6:4:1$. Furthermore, Eq. [1] and Eq. [3] yield the result

$$\frac{s}{1-E} = (2J+1)\frac{\gamma_I}{|\gamma_s|}\left(\frac{W_0 + W_2 + 2W_1 + 2(\nu_1+\nu_2)}{W_2 - W_0}\right), \qquad [6]$$

where the number of electron hyperfine lines has been included in Eq. [6] through the factor $2J + 1$. For the widely used nitroxide radicals such as TEMPO (2,2,6,6-tetramethyl-1-piperidinyloxy), the relevant nuclear spin quantum number is $J = 1$ for ^{14}N, whereas for ^{15}N isotopically enriched nitroxide radicals one has $J = 1/2$.

Equation [6] can be written in a more useful form. Adding and subtracting a term $2W_1 j(\omega_s)$ in the numerator of Eq. [6] one notices from Eqs. [5] that $W_0 + W_2 + 2W_1 j(\omega_s) = R(0)j(\omega_s)$ and $2W_1 = (3/10)R(0)$, where $R(0)$ is the radical-induced nuclear spin–lattice relaxation rate at zero frequency. Furthermore, from Eqs. [5], the denominator can also be written as $W_2 - W_0 = (1/2)R(0)j(\omega_s)$ which, after a few manipulations, leads to the following expression:

$$\frac{s}{1-E} = 2(2J+1)\frac{\gamma_I}{|\gamma_S|}(1/10)\left(7 + \frac{3}{j(\omega_S)}\right) \times \left[1 + \left(\frac{1}{CK(0)T_{10}(0)}\right)\frac{1}{(\frac{1}{10})(7j(\omega_S)+3)}\right]. \qquad [7]$$

In Eq. [7], $1/T_{10}(0) = 2(\nu_1 + \nu_2)$ denotes the intrinsic solvent nuclear spin–lattice relaxation rate at zero frequency. The radical-induced relaxation rate at zero frequency has been written as $R(0) = CK(0)$, where C is the molar concentration of radicals and $K(0)$ is the zero-frequency relaxivity.

Although the right-hand side of Eq. [7] describes the dependence of the enhancement upon molecular motion and free radical concentration through the product ρf, the saturation parameter s on the left-hand side of Eq. [7] may also depend upon the same variables. If irradiation by a rotating magnetic field of amplitude B_2 takes place at the center frequency of one of the hyperfine components one has from Bloch's equations (*6*)

$$s = \frac{\gamma_S^2 B_2^2 T_{1e} T_{2e}}{1 + \gamma_S^2 B_2^2 T_{1e} T_{2e}}, \qquad [8]$$

where T_{1e} and T_{2e} denote electronic spin–lattice and spin–spin relaxation times, respectively.

The mechanisms responsible for ESR linewidths in free radical solutions have been extensively studied (*11*, *12*). In spite of the complexities of the problem, especially when exchange and dipole–dipole interactions between electron spins cannot be ignored, some general statements can be made without going into great detail. The transverse relaxation rate $1/T_{2e} = 1/T'_{2e} + 1/T'_{1e}$ contains a secular term $1/T'_{2e}$ and a lifetime broadening, nonsecular, term $1/T'_{1e}$. For small free radical concentration and low viscosity, both $1/T'_{2e}$ and $1/T'_{1e}$ are often dominated by motion-induced modulation of intramolecular anisotropic interactions (*12*). Thus, in this regime, where we denote the transverse relaxation rate by $1/T_{2e}^{(0)}$, one can expect a saturation parameter s which is independent of free radical concentration although it may depend on viscosity. Hence, from Eq. [7], a linear dependence of $1/(1 - E)$ as a function of $1/C$ should be expected in this regime.

As the free radical concentration is increased, different regimes may become dominant depending upon the concentration level, the viscosity, the value of $T_{2e}^{(0)}$, and the strengths of exchange and dipole–dipole interactions. Following Atkins and Kivelson (*12*) we introduce two parameters denoted by τ_1 and τ_2. They represent the characteristic time two radical molecules spend adjacent to each other and the time between collisions, respectively. Their approximate values can be obtained from the theory of Brownian motion and are given by (*11*)

$$\tau_1 = \pi \eta a_r^3 / kT \qquad [9a]$$

$$\tau_2 = 750 \eta / N_A kTC, \qquad [9b]$$

where a_r represents a spherical equivalent radius of the radical molecule, N_A is Avogadro's number, η is the viscosity, and k is Boltzmann's constant.

A situation of interest for our problem occurs when the exchange interaction between neighboring electron spins just begins to play a role. If the interaction parameter defined as $\alpha^2 = A^2\tau_1^2$, where A is the effective exchange integral, is small ($\alpha^2 \ll 1$) and furthermore $T_{2e}^{(0)} \gg \tau_2 > \tau_1$, the secular linewidth of each hyperfine line begins to increase. A contribution to the width of order $1/T_{2e}^{(e)} = \alpha^2/\tau_2$ has been predicted in this regime (*12*). Thus, from Eqs. [9] one can write for the transverse relaxation rate

$$1/T_{2e} = A\pi^2 N_A a_r^6 \eta C/750kT + 1/T_{2e}^{(0)}, \qquad [10]$$

where the second term in the right-hand side of Eq. [10] does not depend upon the free radical concentration whereas the first term is proportional to the product ηC. It is clear from Eq. [10] that, for a given value of C, the exchange contribution is larger the higher the viscosity η.

Equations [7]–[10] facilitate the study of the various effects which contribute to the enhancement by grouping them into three categories. Dynamical effects due to random molecular motion are described by the viscosity and the reduced spectral density function and are separated from effects caused by the concentration of free radicals. Furthermore, $R(0)T_{10}(0)$ in Eq. [7] is a structure-dependent factor which depends mainly upon internuclear distances and effective "molecular radii" of solvent and free radical molecules.

III. EXPERIMENTAL DETAILS

PEDRI was performed in a homebuilt full-body imaging system operating in a magnetic field of 16 mT (*13*). A "head coil," normally employed for MRI at a proton frequency of 680 kHz, was used as a NMR receiver coil with the irradiation coil for the ESR inside it. The pulse sequence employed in the PEDRI experiments differed from the SE (spin-echo) sequence, used in MRI, only in that it was preceded by a saturating pulse of duration t_w applied within the repetition time interval TR and in that the slice-selection gradient was absent.

The phantoms employed in the PEDRI experiments were 10-mm-diameter tubes filled with approximately 10 ml of TEMPO solutions of various concentrations in solvents with different viscosities. The tubes were placed vertically within a 10-mm-diameter coil made of two turns of silver wire which was tuned and impedance matched to 50 Ω at a frequency of 405 MHz. This corresponds to the lowest frequency hyperfine line of TEMPO in a magnetic field of 16 mT. Enhancements were determined from longitudinal PEDRI profiles through the axis of the cylindrical phantoms.

RF power for ESR irradiation at a frequency of 405 MHz was supplied by Minircuits ZHL-2-12 and ZHL-9000 amplifiers. The power input to the matched load was monitored by a Thruline wattmeter (Bird Electronic Corp.) with power levels

varying between 0.85 and 10.4 W. At the highest power level, some heating was noticed and the steady-state temperature was measured in order to have a more accurate estimate of the viscosity during the PEDRI experiments.

Following Nicholson *et al.* (*8*) we employed glycerol–water mixtures as solvents of controllable viscosity and well-known NMR relaxation mechanisms. The viscosities of two of the glycerol–water mixtures studied were measured at various temperatures using a Brookfirld RVT viscosimeter. At 28°C the measured viscosities were $\eta_1 = 81$ cP (solvent 1) and $\eta_2 = 39$ cP (solvent 2). Solvent 3 was pure water with $\eta_3 = 1$ cP.

PEDRI measurements were performed for various free radical concentrations and the concentration dependences of the enhancements were measured in all three solvents and not only with water as a solvent as in Ref. (*8*). Water solutions of TEMPO were prepared using deionized water equilibrated in air. Freshly prepared concentrated water solutions were next diluted with glycerol until obtaining the desired viscosities and concentrations which ranged between 40 and 0.25 mM.

IV. RESULTS AND DISCUSSION

Figure 1a shows measured values of $1/(1 - E_t)$ as a function of inverse free radical concentration $1/C$ in water–glycerol mixtures of various viscosities. Irradiation power was 10.4 W with $t_w = 1$ s. These data show some agreement with the predictions of Eqs. [7]–[10]. Moreover, they also seem to exhibit some discrepancies which, as will be discussed below, can be quite well understood.

For low concentrations of free radical the data of Fig. 1 exhibit a nearly linear behavior of $1/(1 - E_t)$ with $1/C$ in all three solvents. This agrees with the prediction of Eq. [7] provided that the saturation parameter s can be assumed to be independent of C. However, with increasing free radical concentrations this assumption is expected to break down as the term proportional to ηC in Eq. [10] becomes dominant. This should lead to a crossover from the regime where $1/(1 - E)$ decreases linearly with decreasing values of $1/C$ to one in which it increases with decreasing $1/C$, as observed in Fig. 1. Moreover, these data also confirm that the crossover takes place at a value of C which is lowest for the most viscous solvent, in qualitative agreement with Eq. [10].

From Eqs. [7] and [8] one concludes that the slope of $1/(1 - E)$ as a function of $1/C$ as well as the intercept of the linear portion extrapolated to $1/C = 0$ should both increase as the characteristic correlation time for motion becomes longer. However, the behavior shown by the data in Fig. 1a appears to contradict this prediction. The slope of the linear region corresponding to low free radical concentrations appears to be *larger* for water ($\eta = 1$ cP) than for solvent 2 ($\eta = 39$ cP). Also the enhancements observed for solvent 2 in this region are larger than those for water, although in the high free radical concentration region the situation appears to reverse. Moreover, the enhancements in the low-C region can be seen to be less sensitive than those in the high-C region to a change from the most viscous solvent 1 to water.

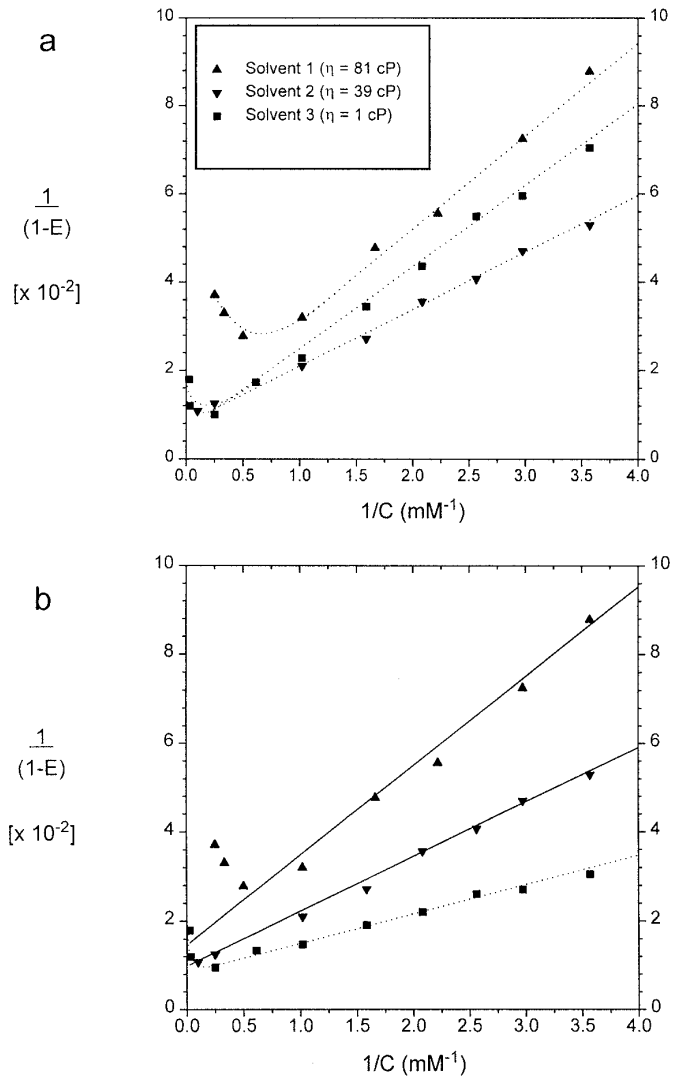

FIG. 1. (a) Values of $1/(1 - E_t)$, as a function of the inverse concentration for TEMPO solutions in three solvents: (▲) solvent 1, (▼) solvent 2, and (■) solvent 3. E_t are values of the enhancements measured with an irradiation time $t_w = 1$ s and an applied RF power of 10.4 W. (b) Values of $1/(1 - E)$ obtained from the data of (a) by correcting for the finite irradiation time. The solid lines are theoretical fits obtained from the dashed line.

These apparently contradictory aspects of the data of Fig. 1 can be understood by examining an operational parameter which appears to play a central role in determining motion-related contrast in PEDRI. From an operational point of view, potential applications of the present imaging scheme, at a field of 16 mT, would almost certainly require field-cycled PEDRI (*14*) where the duration of the ESR irradiation is limited to a finite time interval t_w preceding the acquisition period. This limitation of irradiation time is convenient for various reasons, such as minimizing heating effects and reducing unwanted interference during data acquisition. The electronic magnetiza-

tion transfer time t_w can be seen to strongly influence motion-related contrast in the low free radical concentration region and can therefore be employed as a control parameter.

Since Eq. [7] has been derived from Solomon's equations (*9*) under the assumption of a steady state, whereby the populations of the nuclear Zeeman levels are no longer changing, a correction is needed for a finite magnetization transfer time t_w. In this case, the time-dependent solution of Solomon's equations is required in order to correct the value of $1/(1 - E_t)$, obtained with finite t_w. In this manner it can be shown that multiplication of $1/(1 - E_t)$ by the factor $F(t_w, C) = 1 - \exp(-t_w/T_1) = 1 - \exp[-t_w(1/T_{10} + CK)]$ yields directly the steady-state value $1/(1 - E)$.

In order to check the effect of finite values of t_w, enhancements for all three solvents were measured for various values of t_w at three different concentrations. It was found that for the value $t_w = 1$ s used in Fig. 1a, a correction factor $F(t_w, C) \approx 1$ could be assumed for solvent 2 and solvent 1 over the entire concentration range. For solvent 3, the correction factor was found to be significantly smaller than unity for low values of C and could be described quite closely by the expression

$$F(t_w, C) = 1 - \exp\{-[t_w/T_{10}(0)][1 + CK(0)T_{10}(0)]\}, \quad [11]$$

where the value $T_{10}(0) = 2.65$ s, for water used in our solutions, was determined by an independent measurement in the applied magnetic field of 16 mT. Furthermore the relaxivity $K(0)$ was also determined separately from spin–lattice relaxation measurements in solutions of known free radical concentrations. From these two measurements the value $K(0)T_{10}(0) = 1.8\ (\text{mM})^{-1}$ was found for water solutions of TEMPO.

Figure 1b shows plots of $1/(1 - E)$ obtained from the data of Fig. 1a after correction for the finite electronic magnetization transfer time $t_w = 1$ s employed in these data. Since the condition $\omega_I\tau_0 \ll 1$ is satisfied for all three solvents, the values of T_{10} are expected to be inversely proportional to the correlation times and also to the viscosities. Hence for water, with the lowest viscosity of all three solvents, one has $T_{10}(0)$ (2.65 s) $> t_w$ (1 s), which from Eq. [11] leads to a decreasing enhancement with decreasing concentration. Thus, despite that for water it is possible to assume $j(\omega_s \cong 1$ in Eq. [7], the slope of $1/(1 - E_t)$ as a function of $1/C$ can be larger, in the low free radical concentration region, than that for solvent 2.

For solvents 1 and 2, with much higher viscosities, the condition $T_{10} < t_w$ prevails and the effect of a finite value of t_w is negligible for $t_w = 1$ s as shown in Fig. 1b.

A further check of Eq. [7] for solvent 3 (water), where the condition $j(\omega_s) \cong 1$ prevails, is furnished by the slope of $s/(1 - E)$ as a function of $1/C$ for low C. This slope must

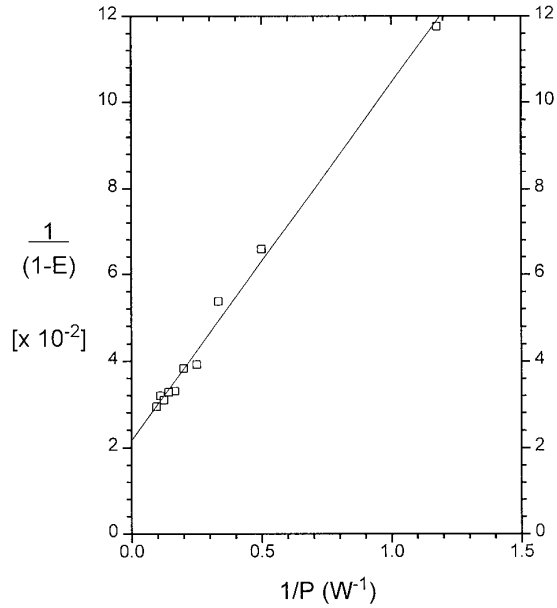

FIG. 2. Values of $1/(1 - E)$ as a function of $1/P$, where P denotes the applied irradiation power for a 0.34 mM water solution of TEMPO.

be consistent with the independently determined value $K(0)T_{10}(0) = 1.8\ (\text{mM})^{-1}$ but its measurement requires a determination of the saturation parameter s. The intercept of the low-C region, straight line portion of $s/(1 - E)$, extrapolated to $1/C = 0$, provides an additional check of Eq. [7], also requiring a measurement of the saturation parameter s.

The saturation parameters s for various values of C and power levels for solvents 1–3 were determined by measuring the enhancement as a function of applied RF power (*6, 8*). From Eqs. [7] and [8] a plot of $1/(1 - E)$ as a function of $1/P$, where P denotes the applied RF power, should yield a straight line. From the intercept of this line, when extrapolated to $1/P = 0$, one can obtain the saturation parameter s for any given power and concentration.

Figure 2 shows a plot of $1/(1 - E)$ as a function of $1/P$ for a water solution of TEMPO with $C = 0.34$ mM. The RF power applied to the resonant circuit at a frequency of 405 MHz ranged from 10.4 to 0.86 W. The data were corrected for the finite duration $t_w = 1$ s of the irradiation pulse, as described earlier.

Figure 3 shows plots of $1/(1 - E_t)$ for water solutions of TEMPO as a function of $1/C$ for two values of the applied power. The larger enhancements correspond to $P = 10.4$ W, whereas the smaller enhancements correspond to $P = 0.86$ W. From the data of Fig. 2, one obtains for the saturation parameters $s(10.4\ \text{W}) = 0.76$ and $s(0.86\ \text{W}) = 0.20$ which enables one to also plot $s/(1 - E)$ in Fig. 3. The correction for $t_w = 1$ s was performed using Eq. [11] for both values of power. The data suggest that $s/(1 - E)$ values obtained with $P = 10.4$ W and $P = 0.86$ W are in good agreement. Moreover, the straight line shown in Fig. 3 is a plot of the

theoretical expression for $s/(1 - E)$ given by Eq. [7] with $j(\omega_s) \approx 1$ neglecting differences in the populations of the hyperfine levels. Hence, a value $2(2J + 1)\gamma_I/|\gamma_s| \approx 1/110$ with $J = 1$ was assumed and the numerical value $K(0)T_{10}(0) = 1.8\ (\text{mM})^{-1}$ was determined from independent measurements as explained earlier. The overall consistency appears to be quite satisfactory.

Although the data of Fig. 3 show that, to a good approximation, the saturation parameter for water solutions of TEMPO is, at least for $C < 4$ mM, only a function of power and not of C, for the more viscous solvents the situation is different. Figure 4 shows values of $1/(1 - E)$ as a function of $1/P$ for solvent 1 at two different free radical concentrations, $C = 0.34$ mM and $C = 2$ mM. From Fig. 4 one obtains saturation parameters $s(10.4\ \text{W}) = 0.5$ for $C = 0.34$ mM and $s(10.4\ \text{W}) = 0.4$ for $C = 2$ mM. This confirms that the crossover in $1/(1 - E)$ observed in Fig. 1 for solvent 1 at $C \approx 2$ mM is actually caused by a decrease of the saturation parameter as suggested by Eqs. [8]–[10].

Finally, the role of the reduced spectral density function, which with increasing viscosity could affect the slopes and the $1/C = 0$ intercepts of the straight lines in the low-C region of Fig. 1b, should be addressed. A specific form of $j(\omega)$, derived from Torrey's theory of relaxation by translational diffusion (*15, 16*), is known to be quite successful in the description of spin–lattice relaxation of pure glycerol in a wide range of temperature and frequency (*16*). The correlation times τ_N obtained from this function have been shown to agree with those

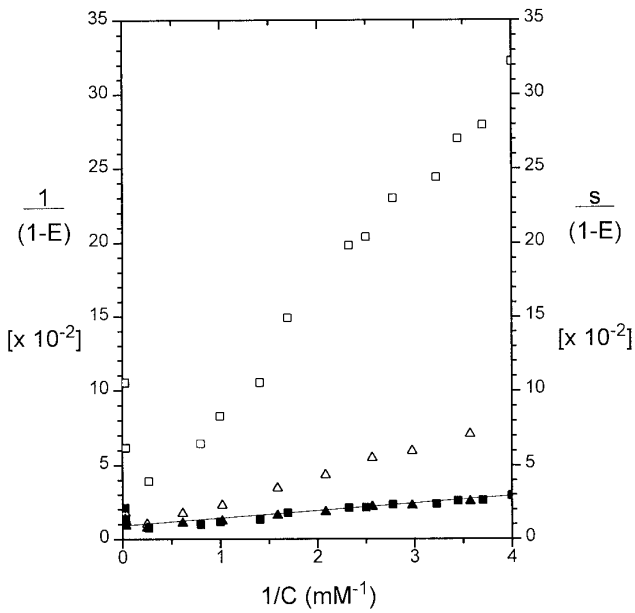

FIG. 3. Values of $1/(1 - E)$ as a function of inverse concentration $1/C$ in water solutions of TEMPO for two values of applied power: (□) 0.86 W and (△) 10.4 W. The data were corrected for the finite irradiation time $t_w = 1$ s employed in the measurements. Also shown are the corresponding values (■) and (▲) of $s/(1 - E)$, where s denotes the previously determined saturation parameters. The straight line is a theoretical prediction.

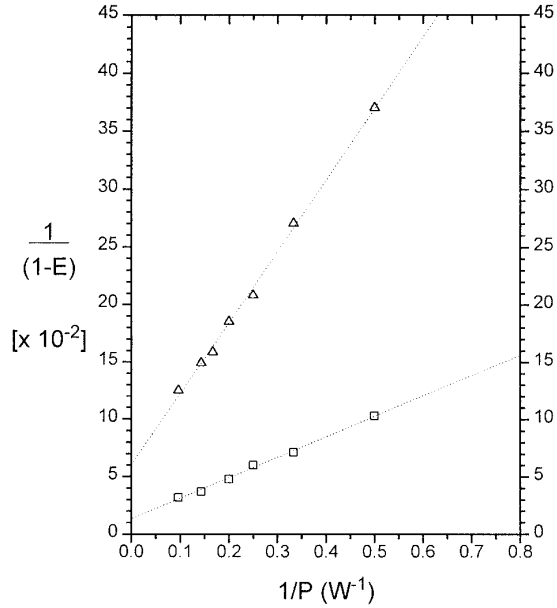

FIG. 4. Values of $1/(1 - E)$ as a function of inverse power $1/P$ for TEMPO solutions in solvent 1 with two different concentrations. (□) $C = 2$ mM and (△) $C = 0.34$ mM.

obtained from dielectric relaxation measurements over a wide range of values (*17*). For $x = \omega\tau_N$, the reduced spectral density function can be written as

$$j(x) = A(x)[B(x) + C(x) + D(x)], \qquad [12]$$

with $A(x) = 3.76/\sqrt{0.5x^5}$, $B(x) = 0.5(x - 1)$,

$$D(x) = B(x)\sin(2\sqrt{0.5x})\exp(-2\sqrt{0.5x}), \qquad [13a]$$

and

$$C(x) = [0.5x + 2\sqrt{0.5x} + 0.5] \times \cos(2\sqrt{0.5x})\exp(-2\sqrt{0.5x}). \qquad [13b]$$

From Eq. [7], the ratio of the $1/C = 0$ intercepts of $1/1 - E$ for solvents 1 and 2, for example, should be given by

$$\Gamma_1/\Gamma_3 = (s_3/s_1)\frac{\left(7 + \dfrac{3}{j(x_1)}\right)}{\left(7 + \dfrac{3}{j(x_3)}\right)}, \qquad [14]$$

with an analogous expression for solvent 2 relative to solvent 3. Here s_3 and s_1 are previously determined values of the saturation parameters, for both solvents in the low-concentration regime.

Although Stokes' law has been shown to be only approxi-

mately valid in glycerol (*18*), it may still be used, in a limited viscosity range, to scale the correlation times. Once a value of $x_1 = \omega_s\tau_N(1)$ is assumed, the value of $x_2 = \omega_s\tau_N(2)$ would then be determined by $\tau_N(2)/\tau_N(1) = \Omega(2)\eta(2)/\Omega(1)\eta(1)$, where $\Omega(1)$ and $\Omega(2)$ denote molecular volumes of solvents 1 and 2, as required by Stokes' law. For solvent 3 ($\eta = 1$ cP) the scaling should be less reliable but, since in this case $x_3 = \omega_s\tau_N(3) \ll 1$ and since values relative to water are treated in Eqs. [14] and [15], the results are not too sensitive to the exact value of x_3 and one may still use Stokes' law. Therefore, once a value of x_1 is assumed, both x_2 and x_3 can be considered to be determined by this scaling.

From Eq. [7], a ratio of the slopes of the linear region of Fig. 1b can also be obtained. It is given by

$$\Sigma_1/\Sigma_3 = (s_3/s_1)\,\frac{\left(7+\dfrac{3}{j(x_1)}\right)}{(7j(x_1)+3)}\,\frac{(7j(x_3)+3)}{\left(7+\dfrac{3}{j(x_3)}\right)} \times \left(\frac{K^{(3)}(0)T_{10}^{(3)}(0)}{K^{(1)}(0)T_{10}^{(1)}(0)}\right), \qquad [15]$$

with an analogous expression for solvent 2 relative to solvent 3.

As mentioned earlier, the ratio $\epsilon_{13} = K^{(3)}(0)T_{10}^{(3)}(0)/K^{(1)}(0)T_{10}(0)$ is a purely geometrical factor whose numerical value can be determined from a fit to the data of Fig. 1b. Moreover, from the theory of nuclear relaxation in liquids, assuming the validity of Stokes' law (*10*) and predominantly rotational diffusive motion in $T_{10}(0)$, one can estimate

$$\bar{\epsilon}_{13} \approx \left(\frac{b_3}{b_1}\right)^6\left(\frac{a_1}{a_3}\right)^2\left(\frac{(1+a_1/a_r)^2}{(1+a_3/a_r)^2}\right).$$

Here b_3 and b_1 denote proton–proton distances in solvents 3 and 1, a_3 and a_1 are the corresponding "molecular radii," and a_r denotes the radius of the radical molecule.

Since solvent 1 and solvent 2 contain 87% (w/w) and 79% (w/w) of glycerol, respectively, it seems reasonable to approximate the ratios $\epsilon_{13} \approx \epsilon_{23}$. Furthermore, using values for pure glycerol relative to water one should obtain an upper limit of ϵ_{13} and ϵ_{23}. Since $\overline{\epsilon_{13}}$ is rather insensitive to changes in the free radical radius we can adopt $a_r \approx 3$ Å, a typical value for nitroxide radicals. Taking $a_1 = 2.49$ Å for pure glycerol, $a_3 = 1.74$ Å for water, $b_3 = 1.58$ Å for the proton–proton distance in water, and $b_1 = 1.78$ Å for the average $b_1 = \langle 1/r_{i,j}^6\rangle^{-1/6}$ involving all proton–proton pair distances in a glycerol molecule, one obtains $\bar{\epsilon}_{13} = 1.7$. If translational diffusion is also included in $T_{10}(0)$ this value would be expected to be approximately 20% higher.

Using x_1 and $\epsilon_{13} = \epsilon_{23}$ as the only two adjustable parameters it is possible to obtain from Eqs. [12]–[15] values of Γ_1/Γ_3, Γ_2/Γ_3, Σ_1/Σ_3, and Σ_3/Σ_3 which fit the experimental data of Fig. 1b. Assuming $\Omega(1)/\Omega(3) \approx \Omega(2)/\Omega(3) = (a_1/a_3)^3 = 2.93$ and using the measured values at 0.34 mM, $s_3(10.4\text{ W}) = 0.76$, $s_1(10.4\text{ W}) = 0.5$, and $s_2(10.4\text{ W}) = 0.7$, one obtains $\Sigma_1/\Sigma_3 = 3.085$, $\Sigma_2/\Sigma_3 = 1.883$, $\Gamma_1/\Gamma_3 = 1.78$, and $\Gamma_2/\Gamma_3 = 1.2$. From Fig. 1b one concludes that, within the experimental accuracy, these values agree quite well with the ratios of the slopes and intercepts relative to water in the linear region of low radical concentrations.

The two parameters found from the fit were $x_1 = 0.47$ and $\epsilon_{13} = \epsilon_{23} = 1.3$; this last value, albeit somewhat lower as expected, is surprisingly consistent with the theoretical estimate for pure glycerol relative to water. From the value of $x_1 = 0.47$, the role of $j(\omega_s)$ can be determined for the data of Fig. 1b. One needs to calculate $j(x_1)$, $j(x_2)$, and $j(x_3)$ given by Eqs. [14] and [15] with the scaled values x_1, x_2, and x_3 which yield correct slopes and intercepts of Fig. 1b. The values found for water were $x_3 = 0.002$ and $j(x_3) = 0.976$, in agreement with the expected condition $\omega_s\tau_N(3) \ll 1$. For solvent 1 (81 cP) we found $x_1 = 0.47$ and $j(x_1) = 0.62$, indicating that in this regime, characterized by the condition $\omega_s\tau_N(1) \approx 1$, an appreciable effect from $j(\omega_s)$ should be present. Finally, for solvent 2 (39 cP) we find $x_2 = 0.226$ and $j(x_2) = 0.732$, suggesting a somewhat smaller effect of $j(\omega_s)$ in this case.

V. CONCLUSIONS

The work of Nicholson *et al.* (*8*), where all measurements with glycerol–water mixtures were performed at a free radical concentration of $C = 2$ mM, has been extended to lower concentrations. This permits a better understanding of the effect of motion upon PEDRI enhancement at low values of C. In this low-concentration regime ($C < 1$ mM in Fig. 1b) the loss of enhancement with increasing viscosity was found to be less severe than at high concentrations ($C > 2$ mM in Fig. 1b). It was also found that the duration of the electronic magnetization transfer time plays a central role in this low-concentration region and could act as a contrast control parameter. Viscosity was found to play a different role at low radical concentrations than at high values of C, especially for short transfer times. Various effects influencing enhancement were separately analyzed and compared with theoretical predictions.

ACKNOWLEDGMENTS

We thank Marcondes Azevedo Matos for able assistance and Constantino S. Yannoni for making available various free radicals. This work was supported by Conselho Nacional de Desenvolvimento Cientifico e Tecnologico and Financiadora de Estudos e Projetos (Brazil).

REFERENCES

1. D. J. Lurie, D. M. Bussel, L. H. Bell, and J. R. Mallard, *J. Magn. Reson.* **76,** 366–370 (1988).

2. D. J. Lurie, I. Nicholson, M. A. Foster, and J. R. Mallard, *Philos. Trans. R. Soc. London A* **333,** 453–456 (1990).

3. D. Grucker and J. Chambron, *Magn. Reson. Imaging* **11,** 691–696 (1993).

4. T. Guiberteau and D. Grucker, *J. Magn. Reson.* **124,** 263–266 (1997).

5. H. Konijnenburg and A. F. Mehlkopf, *J. Magn. Reson. B* **113,** 53–58 (1996).

6. K. H. Hausser and D. Stehlik, "Advances in Magnetic Resonance" (J. S. Waugh, Ed.), Vol. 3, pp. 79–139, Academic Press, New York/London (1968).

7. W. Müller-Warmuth and K. Meise-Gresch, "Advances in Magnetic Resonance" (J. S. Waugh, Ed.), Vol. 11, pp. 1–45, Academic Press, New York/London (1983).

8. I. Nicholson, D. J. Lurie, and F. J. L. Robb, *J. Magn. Reson. B* **104,** 250–255 (1994).

9. I. Solomon, *Phys. Rev.* **99**(2), 559–565 (1953).

10. A. Abragam, "The Principles of Nuclear Magnetism," Chap. 8, Clarendon Press, Oxford (1961).

11. D. Kievelson, *J. Chem. Phys.* **33,** 1094–1106 (1960).

12. P. W. Atkins and D. Kievelson, *J. Chem. Phys.* **44,** 169–174 (1966).

13. G. C. do Nascimento, M. Engelsberg, and R. E. de Souza, *Meas. Sci. Technol.* **3,** 370–374 (1992).

14. D. J. Lurie, J. M. S. Hutchison, L. H. Bell, I. Nicholson, D. M. Bussel, and J. R. Mallard, *J. Magn. Reson.* **84,** 431–437 (1989).

15. H. C. Torrey, *Phys. Rev.* **92,** 962 (1953).

16. F. Noack and G. Preissing, *Z. Naturforsch.* **24,** 143–153 (1969).

17. L. G. Mendes, M. Engelsberg, R. E. de Souza, and I. de Souza, *Phys. Rev. B* **57**(6), 3389–3395 (1998).

18. M. Wolfe and J. Jonas, *J. Chem. Phys.* **71**(8) (1979).